Revista Mexicana de Ingeniería Química

Comparative study: Experimental and simulation data carried out through CFD for the hydrodynamic and mass transfer parameters for pirate acid leaching using ozone as oxidizing agent

Estudio comparativo: Datos experimentales y simulación realizados mediante CFD para los parámetros hidrodinámicos y de transferencia de masa propios de la lixiviación ácida de pirita utilizando ozono como agente oxidante

C. Rodrígurez-Rodrígurez[1], P. Vizguerra-Morales[1], M. Corona-Arroyo[1], L. Alvarado-Montalvo[1],
G. Vázquez-Rodrígurez[2], J. Valtierra-Olivares[1], J.C. Baltazar-Vera[1]*

[1]*Departamento de Ingeniería en Minas, Metalurgia y Geología, División de Ingenierías, Campus Guanajuato, Universidad de Guanajuato, Sede San Matías, Ex-Hacienda San Matías S/N C.P 36050, Guanajuato, Guanajuato, México.*
[2]*Departamento de Ingeniería Civil y Ambiental, División de Ingenierías, Campus Guanajuato, Universidad de Guanajuato, Sede Belen, Juarez 77 C.P 36000, Guanajuato, Guanajuato, México.*

Abstract

In this work is presented a hydrodynamic and mass transfer study using the computational fluid dynamic (CFD) for typical experimental measurements and theoretical calculations for pyrite (FeS_2) dissolution in acid media using ozone as an oxidizing agent, which occurs in a laboratory glass reactor. The hydrodynamics for the reactor employed, was evaluated with the Navier-Stokes equations (κ-ε) RNG turbulence model and the VOF multi-phase model. The results of the hydrodynamic simulation study show that the reactor can operate at a speed range of 1.2 to 4.4 m/s at a total pressure of 12.5 Pa; the Reynolds numerical profile indicates that the flow has a turbulent behavior inside the reactor. For the mass transfer simulation, the model of finite velocity-Eddy dissipation was used for solving the kinetic of the reaction, and was performed for 3 different particle fractions: -106 +75 μm, -38 +25 μm and -25 μm. The simulation results present differences of 17%, 13% and 2% respectively, in comparison with experimental data for pyrite dissolved.

Keywords: pyrite, refractory ores, cyanidation, CFD (computational fluid dynamics), Simulation.

Resumen

En este trabajo se presenta un estudio hidrodinámico y de transferencia de masa utilizando la dinámica de fluidos computacional (CFD) para cálculos teóricos y mediciones datos experimentales correspondiente a la disolución de pirita (FeS_2) en medios ácidos utilizando ozono como agente oxidante, que ocurre en un reactor de vidrio de laboratorio. La hidrodinámica del reactor empleado se evaluó con el modelo de turbulencia RNG propias de las ecuaciones de Navier-Stokes (κ-ε) y el modelo multifase VOF. Los resultados del estudio de simulación hidrodinámica muestran que el reactor puede funcionar a un rango de velocidad de 1,2 a 4,4 m/s a una presión total de 12,5 Pa; el perfil numérico de Reynolds indica que el flujo tiene un comportamiento turbulento dentro del reactor. Para la simulación de transferencia de masa, se utilizó el modelo de velocidad finita-Disipación de Eddy para resolver la cinética de la reacción, y se realizó para 3 fracciones de partículas diferentes: -106 +75 μm, -38 +25 μm y -25 μm. Los resultados de la simulación presentan diferencias de 17%, 13% y 2% respectivamente, en comparación con los datos experimentales de pirita disuelta.

Palabras clave: pirita, minerales refractarios, cianuración, CFD (dinámica de fluidos computacional), simulación.

1   Introduction

The need to study the dissolution of pyrite (FeS_2) is because it is the sulfide mineral most commonly associated with gold., and this is found finely disseminated and encapsulated in the pyritic matrix, and this could not be effectively treated by simple cyanidation. In fact, pyrite needs an oxidant pretreatment such as roasting, pressure oxidation or bacterial oxidation, in order to recover gold in a later stage of cyanidation.

Therefore, oxidation with ozone is presented as an oxidative alternative for the dissolution of pyrite, thus, the knowledge of pyrite behavior generated on the effects of ozone and its by-products is of great interest, for the development of improved technology for the treatment for gold pyrite ores. The application of the computational fluid dynamics (CFD) makes it possible to describe and to support some minerals process that involve complicated physical processes and complex geometry, through numerical solving equations of multiphase fluid motion allows quantitative predictions. Thereby, this prediction allows the optimization for the design of a plant, and minimizes the time and the cost for scaling up from laboratory to full scale. (Cisternas, *et al.*, 2019; Gao and Herbst, 2009). However, the approach for the use of CFD in minerals processing, has been focused on optimizing process, enhancing physical parameters, and validating experimental lab results for some specific systems such as flotation cells (Koh and Schwarz, 2007; Schwarz *et al.*, 2016; Sarhan *et al.*, 2018), hydrocyclones (Rama Murthy and Udaya Bhaskar, 2012; Olson and Van Ommen, 2004; Safa *et al.*, 2014), thickeners (Fawell *et al.*, 2019), electrowinning cells (Mahjabin Najminoori *et al.*, 2015; Leahy and Schwarz, 2010) and heap leaching (Bennett *et al.*, 2012). These works do not present a general application, since the proposed mathematical model depends on the physical and chemical phenomena of the system involved. There are studies that report aspects such as: The effect of some design parameters on the flow fields and energy consumption through CFD simulation (Youcefi *et al.*, 2013); the effect on hydrodynamic parameters when using different eccentric impellers without baffles in a cylindrical tank (Hameur, 2016); the Effects of Baffles on a Vessel Stirred by a Rushton Turbine (Kamla *et al.*, 2017); the hydrodynamic behavior of the agitation of a shear-thinning fluid in a cylindrical vessel (Ameur, 2020); the transitory behavior of CO2 in a gas cooler during variable start-up conditions of a transcritical refrigeration system (Ituna, 2019); the rotating reference frame size for simulating amixing straight-blade impeller in a baffled stirred tank using an MRF approach (De la Concha et.al., 2019). These works show satisfactory evidence that allows to elucidate the viability of the CFD in the analysis of hydrodynamic parameters, which allows proposing this tool to study more complex phenomena such as mass transfer using the appropriate models for this purpose. This study reports the results for a comparative study between experimental and simulated data of the phenomenon of mass transfer for the reactor used for the acid leaching pyrite using ozone presented in previous work (Rodríguez-Rodríguez et. al, 2018), where the stoichiometry (Eq 1) and experimental kinetics parameters obtained were employed at the hydrodynamic validation of a CFD model.

$$2FeS_{2(solid)} + 15O_{3(aqueous)} \longrightarrow 4HSO_4^- + 2Fe^{+3} \atop +H_2O + 2H^+ \qquad + 15O_2 \tag{1}$$
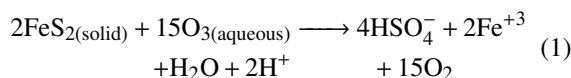
The stoichiometry suggested is the heterogeneous type, which occurs in the solid-liquid interface, where in this system there is no control by diffusion through the layer of solid products on the pyrite particles. In addition, is the first time that a CFD model of pyrite dissolution was addressed in order to validate kinetics parameters obtained in lab tests with ozone and subsequently to propose scalling up from laboratory to full scale dimensions.

2 Materials and methods

With the aim to study the hydrodynamic and the mass transfer for pyrite oxidative dissolution with ozone in acid media is necessary to determine the description of the experimental process (i.e. physical and chemistry parameters), the approach of the mathematical model used and the solution of the case study using CFD simulation.

2.1 Description of the experimental process

2.1.1 Hydrodynamic parameters

Pyrite dissolution was performed in a one-liter cylindrical glass reactor mechanically stirred (Lightnin L1U08) with a radial impeller (radial disk) and hermetically closed with an acrylic cover where 3 electrodes (e.g. pH, ORP and O_3 dissolved electrodes) and 3 components inside (e.g. ozone inlet, sample device and the radial impeller) were coupled (Table 1 and Figure 1). Ozone was generated from dry oxygen with a Pacific Ozone Technology generator (L22) and was fed into to the reactor through a stainless steel cylindrical sparger with a pore opening 5μm.

Table 1. Characteristics and dimensions of the reactor.

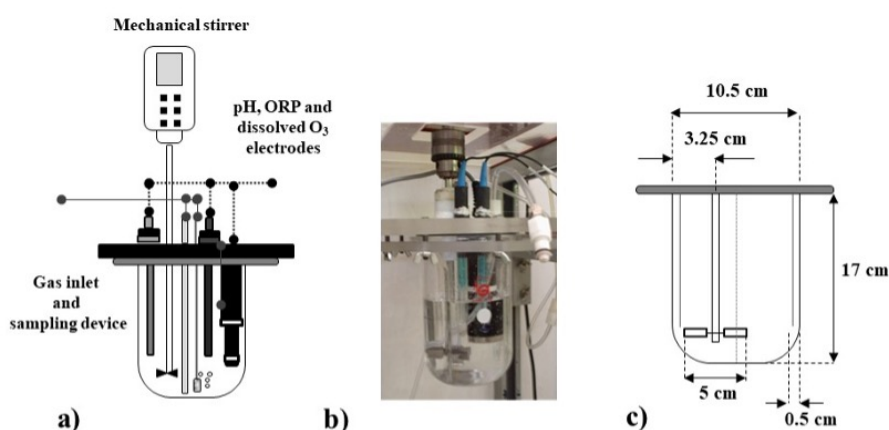| Parameter	Reactor
Internal diameter (m)	0.105
Height (m)	0.17
Volume (m^3)	0.00147
Deflectors	4.0
Shaft diameter (m)	0.01
Shaft height (m)	0.14
Velocity (rpm)	800
Type of impeller	High-shear radial impeller (o Rushton)
Number of blades	6
Impeller diameter (m)	0.0508
Number of components inside	6

Fig. 1. Reactor for the pyrite-ozone reaction a) graphic scheme, b) photograph of the reactor and c) geometry of the stirred experimental reactor.

2.1.2 Mass transfer parameters

For this work, the results obtained in pyrite dissolution (Rodriguez-Rodriguez *et al.*, 2018) for 3 different particle sizes -106 +75μm, -38 +25μm and -25μm were used (e.g. iron dissolved and kinetic constant (k_s)). The experimental conditions for these tests were: 1 g of pyrite, 800 mL of H$_2$SO$_4$ 0.18 M, 1.2 L/min of gas flow rate, 0.079 g O$_3$/L, 800 rpm and 25° C. Table 2 resume the data obtained from pyrite dissolution.

2.2 Approach of the mathematical model for the simulation corresponding to the acid leaching process of pyrite using ozone as an oxidizing agent

The simulation of hydrodynamics and mass transfer was performed with Computational Flow Dynamics tools (CFD) Fluent^{TM} of ANSYS, which allows to simulate parameters of the process such as: the distribution of speed, flow and transfer of mass in the reactor (Gelves *et al.*, 2013). A computer with 8 GB RAM and an AMD A 8 processor was used.

2.2.1 Hydrodynamic study

For the part of hydrodynamics, the equations that are involved in solving the problem to be modeled are the Navier - Stokes equations, (κ-ε) RNG turbulence model wich renormalizes the Navier-Stokes equations, considering the effects of smaller scales of movement that will allow to have more precise results for our equipment, which is laboratory scale (Yakhot et. al, 1992). And the VOF multi-phase model which presents an adequate detail of the bubbles in the two phases, solves the interface by means of the continuity of the equation as a function of the volume fraction and predicts the flow pattern. (Gelves *et al.*, 2013, Guerrero *et al.*, 2017).

Table 2. Experimental data obtained from pyrite dissolution.

	Fe dissolved, mol Particle size fraction		
Time, min	-106 +75μm	-38 +25μm	-25μm
5	0.00010	0.00032	0.00052
15	0.00015	0.00081	0.00158
30	0.00039	0.00165	0.00266
45	0.00057	0.00190	0.00349
60	0.00112	0.00268	0.00435
Kinetic constant, cm/min	0.4	0.4	0.55

Continuity equation

$$\frac{\partial \rho}{\partial t} + \frac{\partial \rho u_x}{\partial x} + \frac{\partial \rho u_y}{\partial y} + \frac{\partial \rho u_z}{\partial z} = 0 \tag{2}$$

Momentum equation in X

$$\frac{\partial u}{\partial t} + u_x \frac{\partial \rho u_x}{\partial x} + u_y \frac{\partial \rho u_x}{\partial y} + u_z \frac{\partial \rho u_x}{\partial z} = \frac{\partial p}{\partial x} + v \left(\frac{\partial^2 u_x}{\partial x^2} + \frac{\partial^2 u_x}{\partial y^2} + \frac{\partial^2 u_x}{\partial z^2} \right) \tag{3}$$

Momentum equation in Y

$$\frac{\partial u}{\partial t} + u_x \frac{\partial \rho u_y}{\partial x} + u_y \frac{\partial \rho u_y}{\partial y} + u_z \frac{\partial \rho u_y}{\partial z} = \frac{\partial p}{\partial y} + v \left(\frac{\partial^2 u_y}{\partial x^2} + \frac{\partial^2 u_y}{\partial y^2} + \frac{\partial^2 u_y}{\partial z^2} \right) \tag{4}$$

Momentum equation in Z

$$\frac{\partial u}{\partial t} + u_x \frac{\partial \rho u_z}{\partial x} + u_y \frac{\partial \rho u_z}{\partial y} + u_z \frac{\partial \rho u_z}{\partial z} = \frac{\partial p}{\partial z} + v \left(\frac{\partial^2 u_z}{\partial x^2} + \frac{\partial^2 u_z}{\partial y^2} + \frac{\partial^2 u_z}{\partial z^2} \right) \tag{5}$$

Turbulent kinetic energy generation equation of the Standard turbulence model (κ-ε) RNG

$$\frac{\partial}{\partial t}(\rho \kappa) + \frac{\partial}{\partial x_i}(\rho \kappa u_i) = \frac{\partial}{\partial x_i}\left[\alpha_\kappa u_{eff} \frac{\partial \kappa}{\partial x_j} \right] + G_\kappa + G_b - Y_M + S_\kappa \tag{6}$$

$$\frac{\partial}{\partial t}(\rho \varepsilon) + \frac{\partial}{\partial x_i}(\rho \varepsilon u_i) = \frac{\partial}{\partial x_i}\left[\alpha_\varepsilon u_{eff} \frac{\partial \varepsilon}{\partial x_j} \right] + C_{1\varepsilon} \frac{\varepsilon}{k} + (G_k + C_{3\varepsilon} G_b) - C_{2\varepsilon} \rho \frac{\varepsilon^2}{k} + S_\varepsilon \tag{7}$$

Turbulent kinetic energy dissipation equation of the standard turbulence model (κ-ε) RNG

$$\mu_t = \mu_{t0} f\left(\alpha_s, \Omega, \frac{k}{\varepsilon} \right) \tag{8}$$

The model's constants, $C_{1\varepsilon}$, $C_{2\varepsilon}$ obtained by the analytical derivation of the RNG theory, yield the values 1.42 and 1.68 respectively. The previous equations were solved by the VOF model for multi-phase mixtures (Jiang *et al.*, 2002), this because there is a stirring of three phases in the reactor, the liquid, solid and gaseous ozone phase. This model solves the equations of continuity, momentum and energy for the mixture and the volume fraction equation for the secondary phases, as well as the algebraic expressions for the relative velocities (Medvitz *et al.*, 2001).
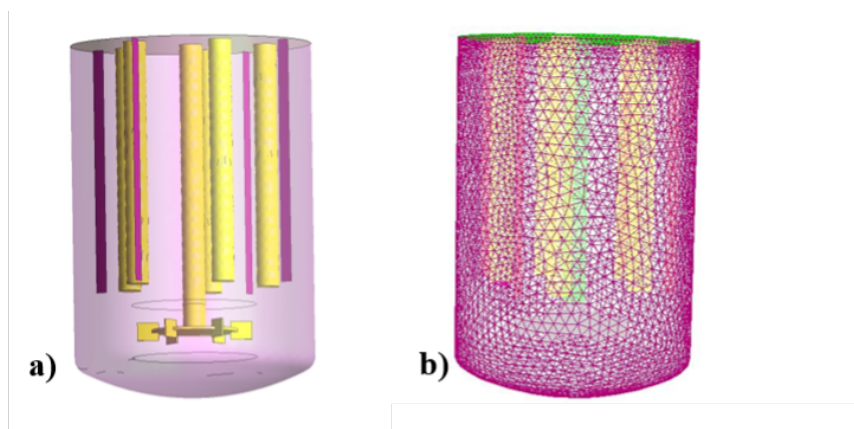
Fig. 2. a) Schematic of the reactor and b) reactor mesh (185568 tetrahedral cells).

For this study the VOF model uses an additional equation as a function of volume fractions for solve the interfaces.

$$\frac{\partial a_i}{\partial t} u_i \nabla (a_i) = 0 \qquad (9)$$

And consider energy field equation (Samkhaniani and Ansari, 2012) wich defined as:

$$\frac{\partial}{\partial t}(\rho C_p T) + \nabla \cdot (\rho C_p U T) = \nabla \cdot (k \nabla T) - m^* h_{LG} \quad (10)$$

$$m^* = \frac{T - T\,sat}{R h_{LG}} \times a_L \nabla a_L \qquad (11)$$

2.2.2 Mass transfer study

In the case of mass transfer, the equations were solved by the model transfer of species solving the kinetics of the chemical reaction by the model of finite velocity - Eddy dissipation; considering 4 species as reactants and 3 species as products, likewise, the coefficients stochymetrics described in the chemical reaction in eq. 1 were used. Experimental data obtained such as the estimated activation energy with a value of 14920 J/mol, a temperature exponent of order 1 and a pre-exponential factor equal to 0.00401 s^{-1} were used (Rodríguez *et al.*, 2018). For the above, the software was used FLUENT 14$^{\text{TM}}$ using the finite volume method (LeVeque, 2004). The equation for the mass flux is shown below:

$$\vec{J} = -\left(\rho D_{i,m} + \frac{\mu_t}{S c_t}\right) \nabla Y_i \qquad (12)$$

The source of chemical species *i* in the reaction are resolved as the sum of the Arrhenius energy generations on the N_R reactions of the participating species;

$$R_i = M_{w,i} \sum_{r=1}^{N_R} \hat{R}_{i,R} \qquad (13)$$

The velocity constant is calculated by Fluent using the expression of Arrhenius;

$$k_{fJ} = A_T T^{\beta_r} e^{E_r/RT} \qquad (14)$$

For this case study, the reaction speed was solved by coupling the Arrhenius expressions to the calculations of the turbulent flows calculated in the hydrodynamics simulation. (Camaño, 2016).
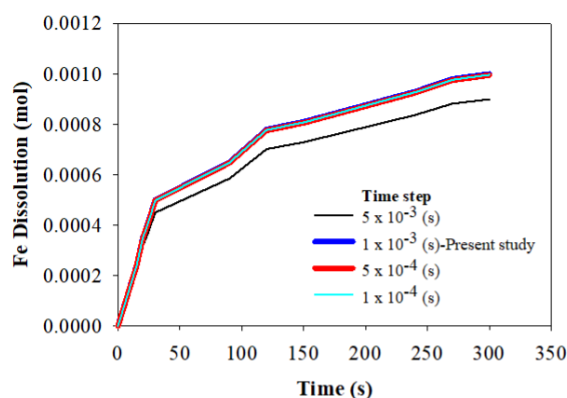

Fig. 3. Sensitivity analysis of the time step.

Table 3. Boundary conditions for the generation of the mesh.

Border condition name	Border condition type
Default - inside	Inside
Default - inside:012	Inside
Ozono inlet	Velocity inlet
Flat baffles 4 wall	Wall
Flat baffles 4 wall shadow	Wall
Radial disk 7 top sh interior	Inside
Radial disk 7 top sh wall	Wall
tank liq top	Wall
tank Wall	Wall
top shaft t outershaft	Wall
Wall	Wall

2.3 Generation of the geometric element and mesh for the simulation process

For the elaboration of the mesh of the reactor and its components a method of construction of Superior - Down geometry was used in GAMBIT, using meshing units of the tetrahedral type (Figure 2a). In order to generate the mesh, the boundary conditions shown in Table 3 were used.

2.4 Resolution by simulation by CFD of the mathematical models corresponding to the hydrodynamics and mass transfer

For the simulation a transient state is considered using decoupled equations in relation to the pressure in a three-dimensional geometry. The model (κ-ε) of two RNG equations was used, using the standard wall functions. The model of transport equations for turbulent kinetic energy (k) and dissipation ratio (ε) was used, using a time of 3600 seconds of simulation. The time step independence of the results (Figure 3) is verified by analyzing 4 different time steps (Ituna *et al.*, 2017), for this study the values 5×10^{-3} s, 1×10^{-3} s, 5×10^{-4} s, 1×10^{-3} s were used. The analysis is based on the case corresponding to the fraction of - 25 μm since it was the case that reported the least difference with respect to the experimental data. It can be seen that the Fe dissolution (mol) values are no longer influenced by the magnitude of the time step when the time step is equal to or less than 1×10^{-3} s. Therefore, the time interval of 1×10^{-3} s is chosen for this study in order to reduce calculation time.

To simulate the rotating motion of the impeller, the sliding mesh approach model was used. This is due to the fact that the impeller is very close to the wall and bottom of the tank, which affects the movement of the fluid and is suitable to carry out the numerical simulation in a transitory state (Tabor *et al.*, 1996).
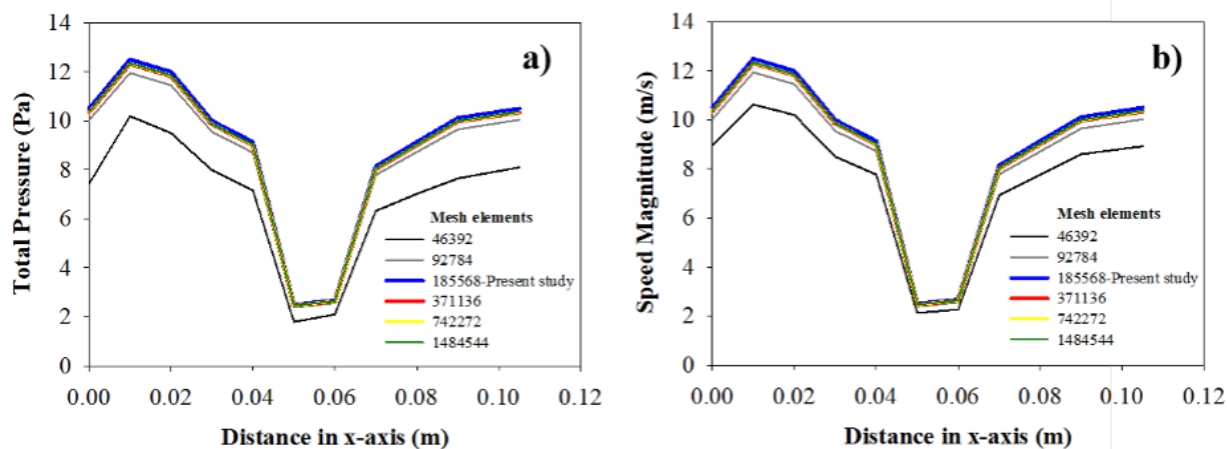

Fig. 4. Mesh independence analysis a) total pressure and b) speed magnitude of the mixture in the reactor.

Table 4. Mesh characteristics of the geometric model.

Item	Size
Nodes	167011
Elements	185568
Orthogonality	
Minimum	0.3542
Maximum	0.9982
Skewness	
Minimum	0.0013
Maximum	0.8314

The calculation starts from values experimentally in the fluid input, carrying the simulation process iteratively until it meets the established convergence criteria (difference less than or equal to 0.001). The discretization of the equations is of second order for the moment equation and the turbulence equations. According to what is recommended by some authors; the mesh tests were performed by increasing the number of cells by a factor of 2 testing a total of 6 cases (Buwa *et al.*, 2006; Ameur, 2016; Ituna *et al.*, 2019). Initially, when going from a mesh of 46392 to 92784 cells, the total pressure (Figure 4a) and speed of the mixture in the reactor (Figure 4b) presented a variation of approximately 15%. Later, when increasing the number of cells from 92784 to 185568, the variation was 4.5%; Likewise, when increasing the number of cells to 371136 the variation was approximately 4.2%; consequently, when increasing the number of cells to 742272 a difference of around 4.18% was registered; Finally, for the case where the number of cells was increased to 1484544, a difference of 4.17% was obtained. These results indicate that for cases from 185568 cells onwards, the difference between them is minimal, which makes it possible to make the decision to use the mesh with 185568 cells in order to reduce the computation time required. Table 4 shows the mesh characteristics of the geometric model.

3 Results and discussion

3.1 Hydrodynamic simulation

Next, results of the simulation corresponding to the hydrodynamics of the leach reactor are presented considering a multiphase model of mixing for 3 phases, gaseous (O_3), solid (FeS_2) and liquid (H_2O, H^+). The results for the simulation of the hydrodynamics include averages of pressure, density

and magnitudes of speed with their corresponding vectors, the following process conditions were used: 880 rpm as agitation speed and ozone injection flow of 1.2 L/min. Figure 5a shows the static pressure contour of the mixture in the reactor, in this figure it can be seen that the pressure varies from 6.3 Pa to 7.5 Pa with an average value of 6.73 Pa.

Figure 5b shows the static pressure profile of the mixture in the reactor, which indicates that there are pressure variations during the process. For the interval of $0 \leq 0.02$ m, there is a decrease in static pressure from 7.5 to 6.3 Pa, which corresponds to the bottom of the reactor, for the interval $0.02 \leq 0.07$ m, the pressure range is located at a constant value of 6.3 Pa, corresponding to the impeller, for the range of $0.07 \leq 0.08$ m own of the section of fluid contact with the shaft of the propeller and the electrodes the pressure increases until reaching a value of 7.0 Pa. With regard to the interval $0.08 \leq 0.11$ m which corresponds to the upper part of the reactor, the pressure increases linearly until a value of 7.5 Pa is registered.

Figure 6b shows the total pressure profile of the mixture in the reactor, showing an increase in pressure in the reactor for the interval $0 \leq 0.02$ m, reaching a value of 12.5 Pa corresponding to the bottom of the reactor, with respect to the impeller section for the position $0.02 \leq 0.07$ m the pressure decreases until reaching a value of 8.15 Pa. For the proper section of the impeller shaft and the electrodes specifically for the position $0.07 \leq 0.08$ m. There is an increase in light pressure until it reaches a value of 9.14 Pa.

In what corresponds to the section of the upper part of the reactor for the position $0.08 \leq 0.11$ m the pressure reaches up to 10.5 Pa. The total pressure contour of the mixture in the reactor indicates that the pressure varies from 2.5 Pa to 12.5 Pa with an average value of 8.83 Pa (Figure 6a). The simulation study indicates that the static and total pressure are in a range of 0 to 12.5 Pa, which is indicative of homogeneity of this parameter, which allows to deduce that the process can be carried to various levels of scaling without changes drastic pressure.

Figure 7a shows the speed magnitude contour of the mixture in the reactor, which indicates that the speed varies in the range of 1.2 to 4.4 m/s, with an average of 3.4 m/s. Figure 7b shows the velocity profile inside the reactor which indicates that there is a decrease in speed for the interval $0 \leq 0.02$ m, reaching a value of 3.59 m/s, which corresponds to the bottom of the reactor, for the impeller section $0.02 \leq 0.07$ m the speed registers a heterogeneous decrease in the reactor until reaching a value of 1.8 m/s.
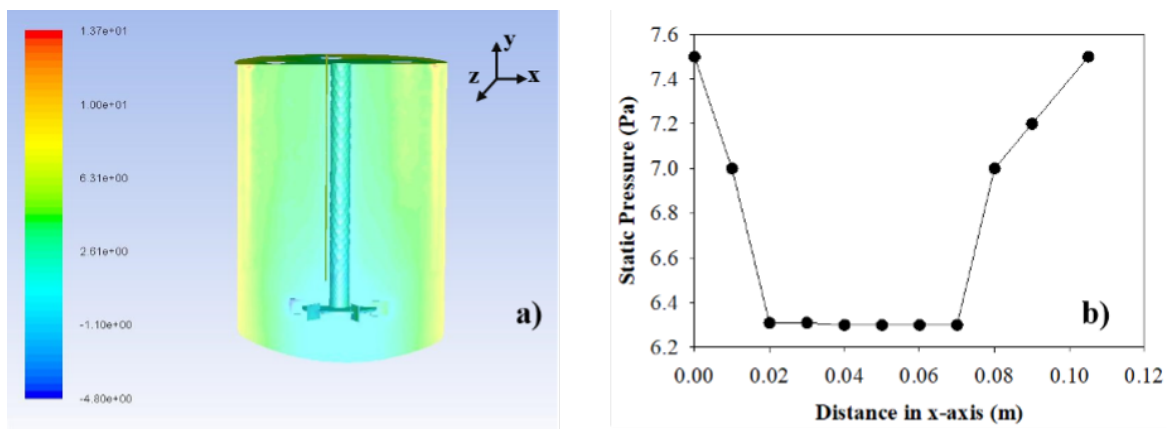
Fig. 5. a) Contour of static pressure of the mixture in the reactor and b) static pressure profile of the mixture in the reactor.
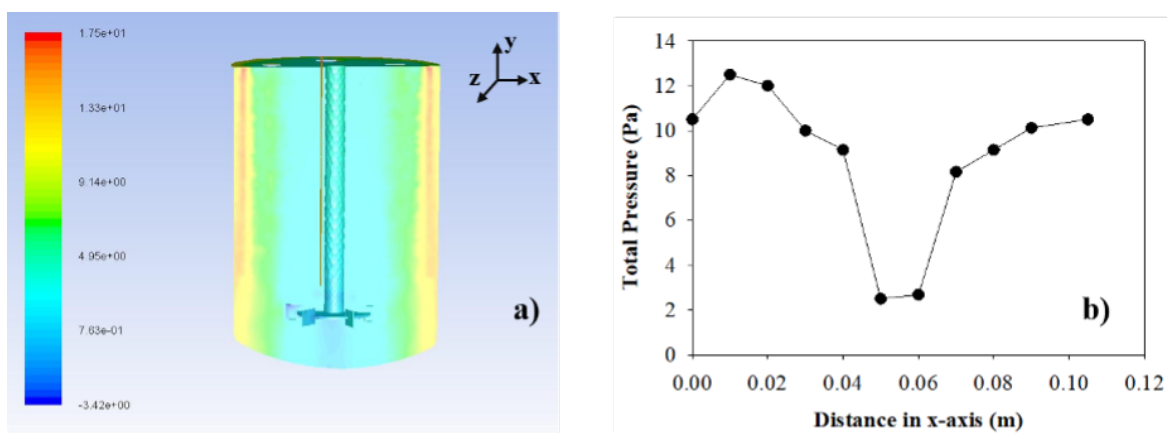

Fig. 6. a) Total pressure contour of the mixture in the reactor and b) profile of total pressure of the mixture in the reactor.
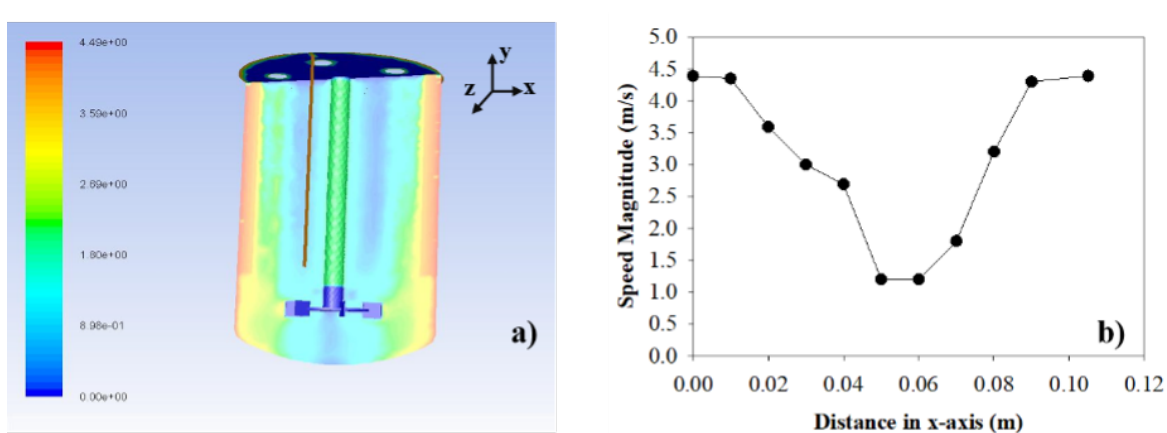

Fig. 7. a) Contour of the speed and b) speed magnitude profile of the mixture in the reactor for 3600 seconds.
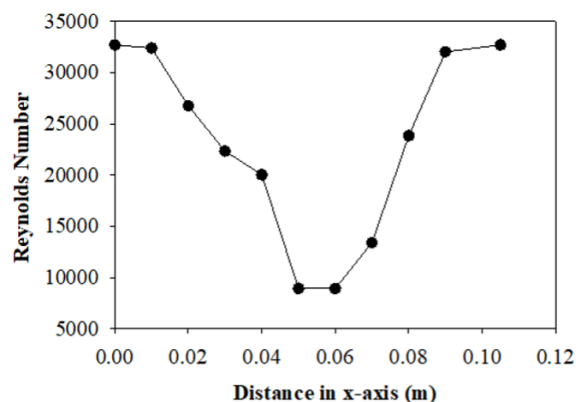
Fig. 8. Reynolds number profile in the reactor for 3600 seconds.

For the interval corresponding to the axis of the impeller that corresponds to 0.07 ≤ 0.08m the speed increases linearly until reaching 3.2 m/s. Finally, for the upper area of the reactor corresponding to 0.08 ≤ 0.11m, there is a tendency of a slight rise in speed until it reaches a value of 4.39 m/s.

Figure 8 shows the Reynolds number profile inside the reactor, this profile indicates that there is a decrease in turbulence for the interval 0 ≤ 0.02 m, reaching a value of 26737.15, corresponding to the bottom of the reactor, with respect to the impeller section 0.02 ≤ 0.07m the turbulence decreases in the first four positions and increases slightly in the position closest to the axis to a value of 13401.85.

For the proper interval of the impeller shaft that corresponds to 0.07 ≤ 0.08m the Reynolds number grows linearly until it reaches 23832.55. Finally, for the upper area of the reactor 0.08 ≤ 0.11m, there is a tendency of slight rise in turbulence until reaching a value of 32695.29. The results of the moment transfer show that although the reactor works in a turbulence regime, the movement of fluid remains constant without sudden changes in speed, which is indicative that the process reaches a hydrodynamic stability and therefore exists viability of scaling it.

3.2 Comparative study of experimental data vs simulation for the mass transfer process for the acid leaching of pyrite using ozone as an oxidizing agent

In this section we present the experimental vs simulation comparison for the process of mass transfer to different particle sizes for the acid leaching of pyrite using ozone as an oxidizing agent, the particle

fractions for this study were: -106 +75 μm, -38 +25 μm y -25 μm.

Figure 9 shows an experimental vs. simulation comparison for the mass transfer process for the acid leaching of pyrite using ozone as an oxidizing agent, using a particle fraction of -106 +75 μm. The value of the kinetic constant (k_s) of 0.4 cm/min was used, which was the one that best fitted the experimental data. In this figure it is observed that for 0 ≤ t ≤ 5 min the generation of the Fe ion increases linearly until reaching a value of 0.0001 mol of Fe for the experimental process and 0.0001267 mol of Fe for the simulation, for 5 ≤ t ≤ 15 min, product generation increased slightly linearly, reporting maximum values of 0.00015 mol Fe for the experimental phase and 0.000129 mol Fe for the simulated process. With regard to the interval 15 ≤ t ≤ 30 min, the generation of the Fe ion increases considerably until reaching values of 0.00039 and 0.00045 mol for the experimental process and the simulation respectively, for 30 ≤ t ≤ 45 the product generation rate remains constant, reporting maximum values of 0.00058 mol of Fe according to the experimental data and 0.00072 mol of Fe for the simulated mechanism. Finally, for the interval 45 ≤ t ≤ 60 min, the generation of the Fe ion reached values of 0.00112 mol and 0.00135 mol for the experimental process and the simulation respectively. The simulation reported values above the experimental ones for the intervals 0 ≤ t ≤ 15 min and 30 ≤ t ≤ 60 min and for the interval 15 ≤ t ≤ 30 min, the experimental data are superior to the simulated ones. The comparison for the particle fraction of -106 +75 μm, indicates that the difference between both ranges between 13% and 21%.
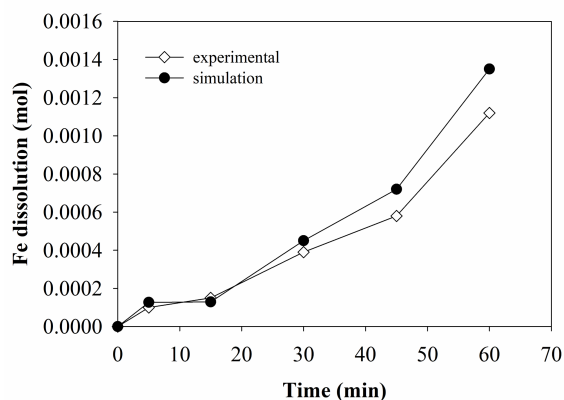

Fig. 9. Experimental and simulation comparison for the mass transfer process for the acid leaching of pyrite using ozone as an oxidizing agent, employing a particle fraction of -106 +75 μm.

Fig. 10. Experimental and simulation comparison for the mass transfer process for the acid leaching of pyrite using ozone as an oxidizing agent, using a particle fraction of -38 +25 μm.
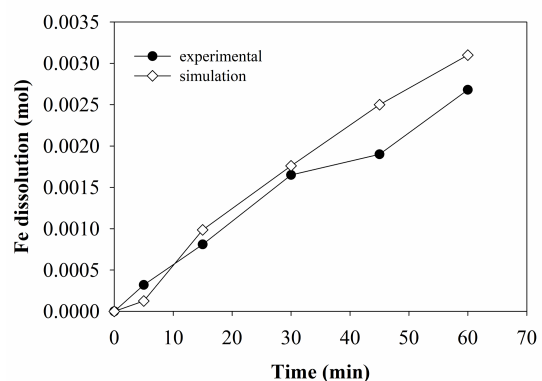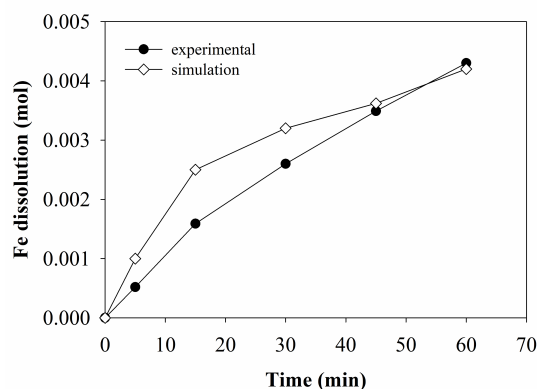

Fig. 11. Experimental and simulation comparison for the mass transfer process for the acid leaching of pyrite using ozone as an oxidizing agent, using a particle fraction of -25 μm.

Figure 10 shows the data corresponding to the fraction -38 +25μm. The value of the kinetic constant (k_s) of 0.4 cm/min was used. This figure shows that for $0 \leq t \leq 5$ min, the generation of the Fe ion increases linearly until reaching a value of 0.00032 mol of Fe for the experimental process and 0.000126 mol of Fe for the simulation, for $5 \leq t \leq 15$ min, the generation of product increased linearly, reporting a maximum value of 0.00081 mol of Fe for the experimental phase and a considerable increase until reaching a value of 0.000986 mol of Fe for the simulated process. With regard to the interval $15 \leq t \leq 30$ min, the generation of the Fe ion increases until reaching values of 0.00165 and 0.00176 mol for the experimental process and the simulation respectively, for $30 \leq t \leq 45$ the rate of product generation continues to increase, reporting maximum values of 0.0019 mol of Fe according to the experimental data and 0.0025 mol of Fe for the simulated mechanism. Finally, for the interval $45 \leq t \leq 60$ min, the generation of the Fe ion reached values of 0.0027 mol and 0.0031 mol for the experimental process and the simulation respectively. The simulation reported values above the experimental ones for the interval $15 \leq t \leq 60$ min and for the interval $0 \leq t \leq 15$ min, the experimental data are superior to the simulated ones. These results, indicates that the difference between the two ranges between 13% and 24%.

Figure 11 shows the data corresponding to the fraction -25 μm. The value of the kinetic constant (k_s) of 0.55 cm / min was used. In Figure 9 it is indicated that for $0 \leq t \leq 5$ min the generation of the Fe ion increases linearly until reaching a value of 0.00052 mol of Fe for the experimental process and 0.0010 mol of Fe for the simulation.

Regarding the interval $5 \leq t \leq 15$ min, product generation increased considerably linearly, reporting a maximum value of 0.0015 mol Fe for the experimental phase and 0.0025 mol Fe for the simulated process. With regard to the interval $15 \leq t \leq 30$ min, the generation of the Fe ion increases until reaching values of 0.0026 and 0.0032 mol for the experimental process and the simulation respectively, for $30 \leq t \leq 45$ the rate of product generation continues to increase, reporting maximum values of 0.0035 mol of Fe according to the experimental data and 0.0036 mol of Fe for the simulated mechanism.

Finally, for the interval $45 \leq t \leq 60$ min, the generation of the Fe ion reached values of 0.0043 mol and 0.0042 mol for the experimental process and the simulation respectively. The results show that the values reported by the simulation and the experimental data are better approximated as the process described in this case study progresses. The comparison using the particle fraction de -25μm, indicates that the difference between the two oscillates between 2% and 48%, the foregoing is indicative that the dispersion range between the experimental data and the simulated data increases in the interval $5 \leq t$ 45 min, which suggests that the adjustment is more successful in the initial and final stage of the process giving a reliable simulation model for these stages.

Conclusions

This CFD model calculation seem to be an appropriated prediction for pyrite leaching using

ozone as an oxidizing agent, when the fundamental underlaying equations used, such as Navier-Stokes equations (κ-ε) and Finite Speed-Eddy Dissipation were fitted for the hydrodynamic and the mass transfer study respectively. The hydrodynamic estimation indicates that a uniform turbulent flow through the leach reactor exists. It can be inferred that the reactor design presents adequate hydrodynamics conditions of pressure and speed in order to operate in a speed range of 1.2 m/s to 4.4 m/s and 12.5 Pa of total pressure, which indicates the feasibility to address the challenges for the modeling a full scale industrial reactor. Three particle size fractions and their kinetics constant were evaluated for the mass transfer process of pyrite dissolution using ozone as the oxidizing agent. For -106 +75 μm fraction, the Fe ion estimated in the simulation was 0.00135 mol, which represents a difference of 17% with respect to the experimental data. The fraction -38 +25 μm, shows that the Fe ion estimated was 0.0031mol, representing a 13% in comparison with the experimental data. Regarding the fraction of -25 μm, presents an estimate of 0.0042 mol of Fe ion that represents 2% difference. These results suggest that the difference between the experimental and simulated data is acceptable for the fraction of particles of -25 μm, while for the cases -106 +75 μm and -38 +25 μm the dispersion increases, which allows to elucidate that at as the particle size increases, the dispersion increases. In the same way, it can be observed that for these same cases as the simulation time of the process increases the dispersion increases, which indicates that the model decreases in precision as the process advances; this allows proposing the convenience of making modifications in terms of simulation parameters that allow obtaining an adequate approximation between experimental and simulated data for this type of case. This contribution reduces experimental times, and so enables rapid analysis by researchers in a possible operating environment for evaluating different scenarios for the use of ozone as an industrial alternative for the treatment of refractory ores that containing a pyritic matrix.

Nomenclature

AT	Frequency of collisions between the molecules of the reagents
a_i	Volume fraction for species i
a_L	Mass fraction of the liquid
β_r	Exponent of reaction temperature

$C_{1\varepsilon}, C_{2\varepsilon}, C_{3\varepsilon}$	Constants
C_p	Heat capacity of the mixture (J/mol-K)
$D_{i,m}$	Coefficient of diffusion for species i (m^2/s).
E_r	Activation energy for the reaction (J/mol).
G_k	Turbulent kinetic energy generation due to speed changes (J).
G_b	Turbulent kinetic energy generation due to vortices (J)
h_{LG}	Latent heat of vaporization of the fluid (J/mol).
k	Thermal conductivity (W/m-K).
$vecJ_i$	Flow of species diffusion i (mol/m^{2}s).
k_{fJ}	Constant of non-reversible speed for reaction.
$M_{w,i}$	Molecular weight of species i (g/mol).
N_R	Number of reactions
p	Average pressure (N/m^2).
R	Universal gas constant (J/mol-K).
$\hat{R}_{i,R}$	Arrhenius molar velocity of creation / destruction (mol/s).
R_i	Rate of creation of species (m/s).
Sc_t	Schmidt number.
S_k	Generation of external turbulence (J).
S_ε	Increased turbulent dissipation (J).
T	Mixing temperature
T_{sat}	Saturation temperature
t	Time (s)
u	Total fluid velocity
u_i	Total fluid velocity for species i (m/s).
u_x	Fluid velocity in the direction x (m/s).
u_y	Fluid velocity in the direction y (m/s).
u_z	Fluid velocity in the direction z (m/s).
u_{eff}	Effective fluid viscosity (Kg/ms)
Y_M	Turbulent speed contributions due to dissipation.
Y_i	Concentration of species i (mol/m^3).

Greek symbols

α_s	Constant of the turn.
α_k	Lock coefficient of turbulent kinetic energy generation.
α_ε	Lock coefficient of turbulent kinetic energy dissipation.
ε	Dissipation per unit of mass (m^2/s^2).
ρ	Density of the fluid in the reactor (kg/m^3).
ν	Kinematic viscosity of the fluid in the reactor (m^2/s).

μ_t Viscosity of fluid turbulence in the reactor (kg/ms).

k Turbulent kinetic energy (J).

μ_{to} Turbulent viscosity (Kgm/s^2).

Ω Characteristic number of the turn.

Acknowledgements

References

Ameur, H., (2016). 3D hydrodynamics involving multiple eccentric impellers in unbaffled cylindrical tank. *Chinese Journal of Chemical Engineering 24*, 572-580. https://doi.org/10.1016/j.cjche.2015.12.010

Ameur, H., (2020). Investigation of the Performance of V-cut Turbines for Stirring Shear-thinning Fluids in a Cylindrical Vessel. *Periodica Polytechnica Mechanical Engineering 64*, 207-211. https://doi.org/10.3311/PPme.13359

ANSYS, Inc., (2013), ANSYS Fluent User's Guide. Canonsburg, PA, USA. Bennett, C. R., McBride, D., Cross M., Gebhardt, J. E., (2012). A comprehensive model for copper sulphide heap leaching: Part I basic formulation and validation through column test simulation. *Hydrometall 127*, 150-161. https://doi.org/10.1016/j.hydromet.2012.08.004

Buwa, V., Dewan, A., Nassar, A.F., Durst, F., (2006). Fluid dynamics and mixing of single-phase flow in a stirred vessel with a grid disc impeller: Experimental and numerical investigations. *Chemical Engineering Science. 61*, 2815-2822. https://doi.org/10.1016/j.ces.2005.10.066

Camaño Camaño, A., (2016). Desarrollo de una metodología mediante CFD para el proceso de combustión en una bomba a volumen constante. *Tesis de Maestría, Universidad de Valladolid*, 12-31.

Cisternas, L. A., Lucay, F. A., Botero, Y. L., (2019). Trends in modeling design, and optimization

of multiphase systems in minerals processing. *Miner. 10*, 1-28. https://doi.org/10.3390/min10010022

De La Concha, A. D., Ramírez, J., Márquez, V.E., Haro, C., Alonso, A.R., (2019). Effect of the rotating reference frame size for simulating a mixing straight-blade impeller in a baffled stirred tank. *Revista Mexicana de Ingeniería Química. 18*, 1143-1160. http://www.rmiq.org/ojs311/index.php/rmiq/article/view/594/187

Fawell, P. D., Nguyen, T. V., Solnordal, C. B., Stephens, D. W., (2019). Enhancing gravity thickener feedwell design and operation for optimal flocculation through the application of computational fluid dynamics. *Miner. Process. and Extr. Metall. Rev.* 1-15. https://doi.org/10.1080/08827508.2019.1678156

Gao, D., Herbst, J. A., (2009). Alternative ways of coupling particle behavior with fluid dynamics in minerals processing. *Int. J. of Comput. Fluid Dyn. 23*, 109-118. https://doi.org/10.1080/10618560902754932

Gelves R, Benavides A, Quintero, J. C., (2013). Predicción del comportamiento hidrodinámico en el escalado de un reactor de tanque agitado para procesos aerobios, mediante CFD. Ingeniare. *Revista Chilena de Ingeniería. 12*, 347-361. http://dx.doi.org/10.4067/S0718-33052013000300005

Guerrero, E., Muñoz, F., Ratkovich, N., (2017). Comparison between eulerian and vof models for two-phase flow assessment in vertical pipes. *Journal of oil, gas and alternative energy sources. 7*, 73-84. http://www.scielo.org.co/pdf/ctyf/v7n1/0122-5383-ctyf-7-01-00073.pdf

Ituna, J.F., Belman, J.M., Elizalde, F., García, O., (2017). Numerical investigation of CO2 behavior in the internal heat exchanger under variable boundary conditions of the transcritical refrigeration system. *Applied Thermal Engineering. 115*, 1063-1078. https://doi.org/10.1016/j.applthermaleng.2017.01.042

Ituna, J.F., Belman, J.M., Elizalde, F., Pérez, V., García, O., Carvajal, I., (2019). Numerical

analysis of CO2 transient behavior in the gas coolerduring variable start-up conditions of a transcritical refrigeration system. *Revista Mexicana de Ingeniería Química. 18*, 3, 1101-1118. http://www.rmiq.org/ojs311/index.php/rmiq/article/view/271/186

Jiang. Y, Khadilkar M, Al-Dahhan M., Dudukovik, M. P., (2002). CFD of multiphase flow in packed-bed reactors: I. k-Fluid modeling issues, fluid mechanism and transport phenomenon. *AIChE J. 48*, 701-715. https://doi.org/10.1002/aic.690480406

Kamla. Y., Bouzit, M., Ameur, H., Arab, M., Hadjeb, A., (2017). Effect of the Inclination of Baffles on the Power Consumption and Fluid Flows in a Vessel Stirred by a Rushton Turbine. *Chinese Journal of Mechanical Engineering. 30*, 1008-1016. https://doi.org/10.1007/s10033-017-0158-5

Koh, P.T.L., Schwarz, M.P., (2007). CFD model of a self-aerating flotation cell. *Int. J. of Miner. Process. 85*, 16-24. https://doi.org/10.1016/j.minpro.2007.08.006

Leahy, M. J., Schwarz, P., (2010). Experimental validation of a computational fluid dynamics model of copper electrowinning. *Metall. and Material. Trans. B. 41B,* 1247- 1260. https://doi.org/10.1007/s11663-010-9432-y

LeVeque R.J., (2004). *Fin Volume Methods for Hyperbolic Problems*. Cambridge University Press, Cambridge, United Kingdom. 31, 64-85.

Mahjabin N., Ali M., Babak G., Shahram D., (2015). CFD simulation of an industrial copper electrowinning cell. *Hydrometall. 153*, 88-97. https://doi.org/10.1016/j.hydromet.2015.02.005

Medvitz R. B., Kunz R. F., Boger D. A., Lindau J. W., Yocum A. M., (2002). Performance analysis of cavitating flow in centrifugal pumps using multiphase CFD. *J. of Fluids Eng. 124*, 377-383. https://doi.org/10.1115/1.1457453

Olson, T.J., Van Ommen, R., (2004). Optimizing hydrocyclone design using advanced CFD model. *Miner. Eng. 17*, 713-720. https://doi.org/10.1016/j.mineng.2003.12.008

Rama Murthy, Udaya Bhaskar, K., (2012). Parametric CFD studies on hydrocyclone.

Powder Technol. 230, 36-47. https://doi.org/0.1016/j.powtec.2012.06.048

Rodríguez-Rodríguez, C., Nava-Alonso, F., Uribe-Salas, A., (2018). Pyrite oxidation with ozone: stoichiometry and kinetics. *Can. Metall. Q. 57*, 294-303. https://doi.org/10.1080/00084433.2018.1460437

Safa, Raziyeh, Soltani Goharrizi, Ataallah, (2014). CFD simulation of an industrial hydrocyclone with Eulerian-Eulerian approach: A case of study. *Int. J. of Min. Sci. and Technol. 24*, 643-648. https://doi.org/10.1016/j.ijmst.2014.07.010

Samkhaniani, N., Ansari, M., (2012). A VOF Method to Phase Change Modeling. *1th Iranian Conference on Heat and Mass Transfer, 1-5.*

Sarhan, A. R., Naser, J., Brooks, G., (2018). CFD model simulation of bubble surface area flux in flotation column reactor in presence of minerals. *Int. J. of Min. Sci. and Technol. 28*, 999-1007. https://doi.org/10.1016/j.ijmst.2018.05.004

Schwarz, M.P., Koh, P.T.L., Verrelli, D.I., Feng, Y., (2016). Sequential multiscale modelling of mineral processing operations, with application to flotation cells. *Miner. Eng. 90*, 2-16. https://doi.org/10.1016/j.mineng.2015.09.021

Tabor, G., Gosman, A.D., Issa, R., (1996). Numerical simulation of the flow in a mixing vessel stirred by a Rushton turbine. *Inst.Chem. Eng. Symp. Ser. 140*, 25-34. http://citeseerx.ist.psu.edu/viewdoc/download?doi=10.1.1.45.7691&rep=rep1&type=pdf

Yakhot, V., Orszag, S.A., Thangam, S., Gatski, T.B., Speziale, C.G. (1992), Development of turbulence models for shear flows by a double expansion technique, *Physics of Fluids A 4*, 1510-1520. https://apps.dtic.mil/dtic/tr/fulltext/u2/a240395.pdf

Youcefi, S., Bouzit, M., Ameur, H., Kamla, Y. and Youcefi, A., (2013). Effect of some design parameters on the flow fields and power consumption in a vessel stirred by a rushton turbine. *Chemical and Process Engineering 34*, 293-307. https://doi.org/10.2478/cpe-2013-0024